A Post-CMOS Micromachined Lateral Accelerometer

Hao Luo, Gang Zhang, L. Richard Carley, *Fellow, IEEE*, and Gary K. Fedder

***Abstract*—In a post-complementary metal–oxide–semiconductor (CMOS) micromachining technology, the process flow enables the integration of micromechanical structures with conventional CMOS circuits which are low-cost and readily available. This paper presents a lateral capacitive sensing accelerometer fabricated in the post-CMOS process. Design advantages include electrically isolated multimetal routing on microstrctures to create full-bridge capacitive sensors, and integration to increase transducer sensitivity by minimizing parasitic capacitance. In a size of 350 μm by 500 μm, this accelerometer has a 1 mG/$\sqrt{\text{Hz}}$ resolution and a linear range of at least $\pm$13 G. The fundamental limitations of mechanical and electronic noise for acceleration sensing are addressed. [709]**

***Index Terms*—Accelerometer, complementary metal–oxide–semiconductor (CMOS), MEMS.**

I. Introduction

OVER the past decade, MEMS technology has been established as a solution for acceleration sensing problems [1]–[5]. Current technologies include two main trends, bulk and surface (thin-film) micromachining. Bulk micromachined devices normally have better noise performance, but they are more expensive than the surface micromachined devices. For those applications that do not require extremely high noise performance such as airbag accelerometers, tilt sensors, computer input interfaces, and virtual reality tracking systems, thin-film devices are quite competitive. Thin-film CMOS micromachining has many attractive features for the fabrication of integrated inertial sensors. The compatibility of the micromachining process with standard CMOS has the advantages of low cost and compact integration of the micromechanical structures and circuits. The close coupling between the sensing element and signal processing circuits reduces the parasitic capacitance, and noise pick-up. Usually at dimensions of 1.2 μm up to 600 μm, CMOS surface microstructures fit in a small die area with circuits placed up to 15 μm from the structures. This means an array of sensing elements can be integrated to overcome the limitations of systems with only a single micromechanical device.

This paper begins with a brief overview of the CMOS-MEMS process developed at Carnegie Mellon University [6], [7]. The physical limitation of sensing elements as well as the interface circuits are discussed. Highlighted issues include a design methodology using curl matching and the CMOS-MEMS quality factor relation with pressure. To improve the performance such as stability, dynamic range and linearity, analog force-feedback with compensation is introduced.

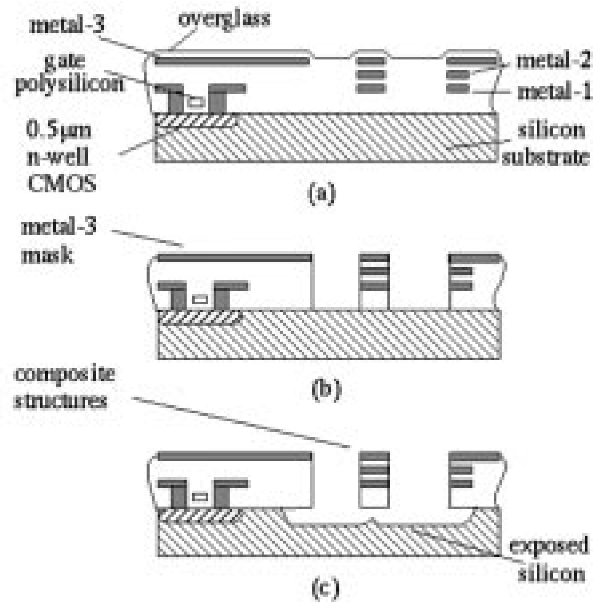

Fig. 1. CMOS-MEMS process. (a) CMOS chip after fabrication. (b) Anisotropic RIE removes dielectric. (c) Isotropic RIE undercuts silicon substrate.

II. CMOS Micromachining Process

The accelerometer described in this paper uses high-aspect-ratio post-complementary metal–oxide–semiconductor (CMOS) micromachining technology [6], [7]. It is fabricated in the Agilent three-metal 0.5 μm n-well CMOS process through MOSIS. After the foundry fabrication, two dry etch steps, shown in Fig. 1, are used to define and release the structure. Fig. 1(a) shows the cross section of the chip after regular CMOS fabrication. In the first step of post processing [see Fig. 1(b)], dielectric layers are removed by an anisotropic CHF_3/O_2 reactive-ion etch (RIE) with the top metal layer acting as an etch resistant mask. After the sidewall of the microstructure is precisely defined, an isotropic SF_6/O_2 RIE is performed to etch away the bulk silicon and release the composite structure [see Fig. 1(c)]. Layout in the metal layers is designed to form beams, plates, and electrostatic comb fingers. Material property values for the composite structures include a density of 2300 kg/m^3 and a Young's modulus of 62 GPa [8].

The availability of CMOS and simple dry-etch micromachining provides a low-cost way to integrate MEMS with

Manuscript received June 12, 2001; revised December 20, 2001. This work was supported by the Defense Advanced Research Projects Agency, Air Force Material Command, USAF, under Agreement F30602-97-2-0323. Subject Editor G. Stemme.

H. Luo, G. Zhang, and L. R. Carley are with the Department of Electrical and Computer Engineering, Carnegie Mellon University, Pittsburgh, PA 15213-3890 USA.

G. K. Fedder is with the Department of Electrical and Computer Engineering and The Robotics Institute, Carnegie Mellon University, Pittsburgh, PA 15213-3890 USA.

Publisher Item Identifier S 1057-7157(02)04983-1.

1057-7157/02$17.00 © 2002 IEEE

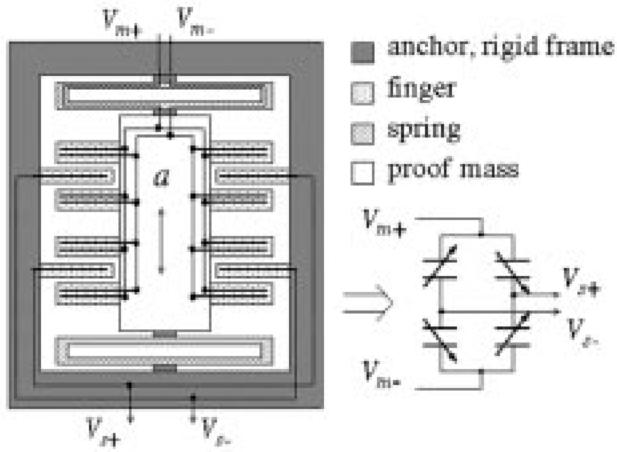

Fig. 2. Schematic of accelerometer and its equivalent model.

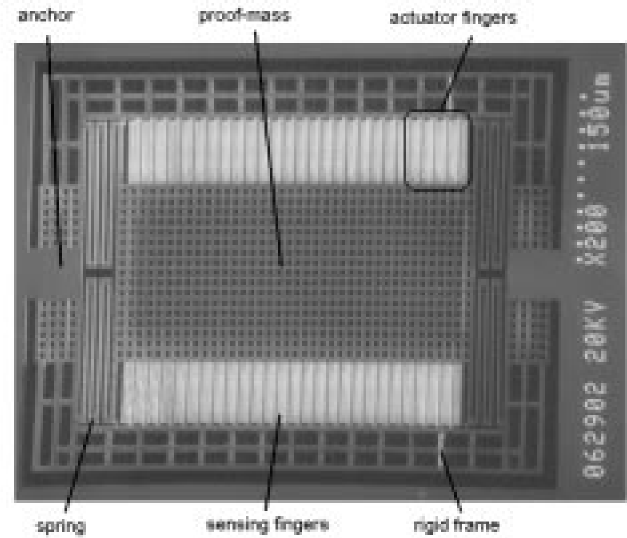

Fig. 3. Scanned electron microscopy (SEM) of released CMOS-MEMS accelerometer.

electronics. Electrically isolated multi-layer conductors can be routed in the composite structures, enabling more design options (compared to homogeneous conductor structures). For example, electrically decoupled sensing and actuating comb fingers may be built on the same structure, and full-bridge capacitive differential and common-centroid comb-finger designs can be readily implemented. A full-bridge capacitive sensor has double transducer sensitivity of a half-bridge. Higher transducer sensitivity improves the signal-to-electrical noise ratio. At the same time, since the full-bridge capacitive sensor has differential output, it has better ability to reject common mode noise. The undercut of silicon in the release step [see Fig. 1(c)] constrains the placement of sensing circuits to at least 15 μm away from the microstructures. Compared to most commercialized polysilicon micromachining technology, the MEMS to electronics interconnect in CMOS-MEMS is shorter, and suffers less parasitic capacitance. Such parasitics on high-impedance wiring can be made small relative to input capacitance of interface circuits, so the transducer sensitivity is larger when capacitive sensing is employed.

The main disadvantage of this process is the out-of-plane and in-plane curling of the composite structures. This curling is caused by the different residual stress of the various oxide and aluminum layers. The out-of-plane curling can be compensated by curl-matching techniques [9] or thermal control methods [10]. The primary cause of in-plane curl is misalignment of the embedded metal layers within thin beams. The in-plane curling can be alleviated by decreasing the beam length or increasing the beam width. The current design has a beam width of 2.1 μm and length of 117 μm, which can exhibit substantial in-plane curl.

III. Acceleration Sensor Design

The sensor transfers the position change into capacitive variation to detect acceleration. It is composed of a proof mass, suspending serpentine springs and comb fingers. The schematic view of the accelerometer is shown in Fig. 2. Using the multi-layer routing technique, this accelerometer has a fully differential topology described in [9]. In the layout, each half-capacitive bridge is split into two parts and located at two cross-axis corners. This differential layout topology cancels common-mode input noise such as substrate coupling, power supply coupling and cross-axis excitation. Since there are multiple sensors and circuitry integrated on the same substrate, coupling through the substrate are to be minimized when high impedance sensing (capacitive sensing) is used. All the signals on the moving part are routed through the multi-layer suspending springs and all the cross links are placed in the proof mass layers. Compared to a polysilicon accelerometer, multi-layer microstructures give more freedom in MEMS design such as creating differential topologies and nested electrostatic driving and sensing [11].

A released accelerometer is shown in Fig. 3. The total device size is 350 μm by 500 μm and the front-end circuitry takes an area of 220 μm by 200 μm (not shown), which is covered by the top metal layer for protection during the micromachining process steps. The accelerometer has a proof-mass of 160 μm by 350 μm with multiple 6 μm by 6 μm releasing holes. The 40 sensing fingers and 12 actuating comb fingers are the same size of 55 μm long and 3.9 μm wide. Each serpentine spring has two turns and the beam in each turn is 117 μm long and 2.1 μm wide. The whole released structure is uniformly 5 μm thick.

The composite structure experiences larger vertical stress gradients than its polysilicon counterpart. Vertical residual stress gradients in the CMOS structures can result in a radius of curvature of 1 mm to 5 mm [12]. Out-of-plane curling can significantly reduce the sidewall capacitance which is critical to capacitive sensing. To solve this problem, fingers on the stator side are attached to a rigid frame (see Fig. 4) instead of to the substrate. The rigid frame is anchored along a common axis with the proof mass, and is subjected to the same stress gradient as the inner structure. Thus, a first-order curl matching can be achieved. To get optimal sidewall alignment, a local matching technique has been developed. The middle part of the rigid frame has the same density of holes in its structure as the proof mass. The outer part of the rigid frame is composed of beams that have the same cross section as the fingers. This design eliminates the pattern-sensitive mismatch between the inner and outer structures.

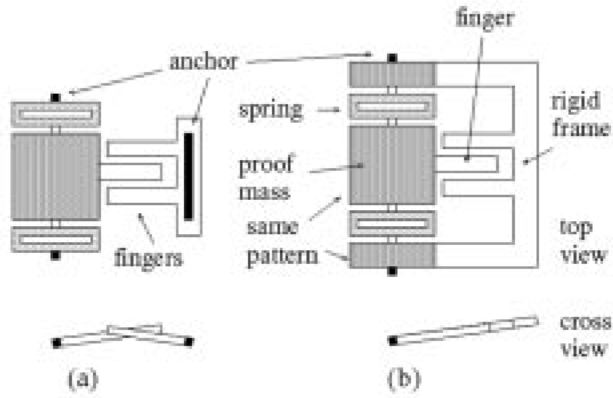

Fig. 4. Local curl matching technique. (a) Without curl matching. (b) With curl matching.

Out-of-plane curl measured with a Wyco NT3300 optical profilometer is shown in Fig. 5. The maximum out-of-plane curl is 6 μm while the mismatch between the rotor and stator fingers is reduced to 0.3 μm.

The proof mass is suspended by serpentine springs (see Fig. 6). The sense-axis spring constant is given by [17]

$$k = \frac{48EI_{zl}[5(\tilde{c}+l)-l)]}{4l^2[5(3\tilde{c}^2+4\tilde{c}l+l^2)+3\tilde{c}^2-l^2]} \tag{1}$$

$$I_{zl} = tW_l^3/12 \tag{2}$$

$$\tilde{c} = dI_{zl}/I_{zd} = dW_l^3/W_d^3 \tag{3}$$

where t is the beam total thickness of 5 μm, l is the long beam length of 117 μm, d is the short beam length of 5.1 μm, W_l (2.1 μm) and W_d (5.1 μm) is the long beam and short beam width, respectively, and E is the composite structure effective Young's modulus of 62 GPa, which is extracted from measurements of cantilever test structures [12]. The spring constant is 1.77 N/m. The only differences in the composite beam mechanical design, compared to polysilicon or silicon beam design, are the values of effective mass density, effective Young's modulus and geometry.

Springs can be attached to the proof mass at its midpoint [see Fig. 6(c)] or at the four corners [see Fig. 6(d)]. The midpoint attachment has good linear motion in plane, but the curling makes it sensitive to tilt with respect to the center line [see Fig. 6(b)]. The corner attachment design avoids the problem with tilting and provides better curl matching.

The accelerometer can be simplified as the lumped parameter model shown in Fig. 7. The differential equation of displacement x as a function of input acceleration a is given by

$$m\frac{d^2x}{dt^2} + b\frac{dx}{dt} + kx = ma_{\text{ext}}. \tag{4}$$

Taking the Laplace transformation gives the system transfer function as

$$H(s) = \frac{X(s)}{A(s)} = \frac{1}{s^2 + s\frac{b}{m} + \frac{k}{m}} = \frac{1}{s^2 + s\frac{\omega_r}{Q} + \omega_r^2} \tag{5}$$

where ω_r is the resonant frequency, b is damping coefficient and Q is the quality factor ($Q = \omega_r m/b$). For most applications, the applied acceleration frequency is much less than ω_r, thus the mechanical sensitivity of the device is $1/\omega_r^2$.

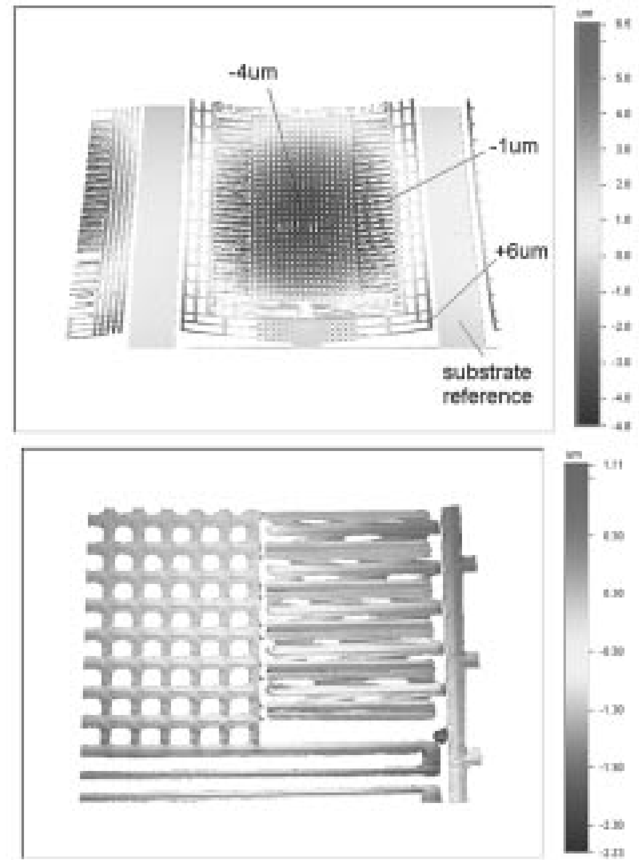

Fig. 5. Optical profilometer measurement showing out-of-plane curl and the curl matching.

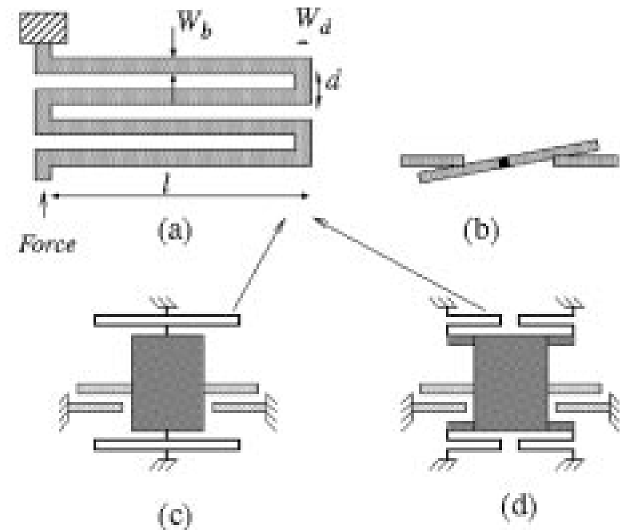

Fig. 6. Spring design. (a) Serpentine spring. (b) Structure tilt. (c) Center attachment. (d) Corner attachment.

By detecting the sidewall capacitance change between the comb fingers attached to the proof mass and anchor, lateral motion and therefore acceleration is measured. Shown as Fig. 8, the three metal layers in each finger are connected together as one

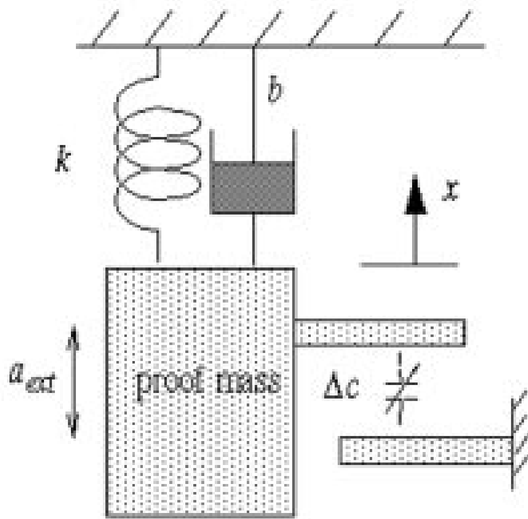

Fig. 7. Lumped parameter model of accelerometer.

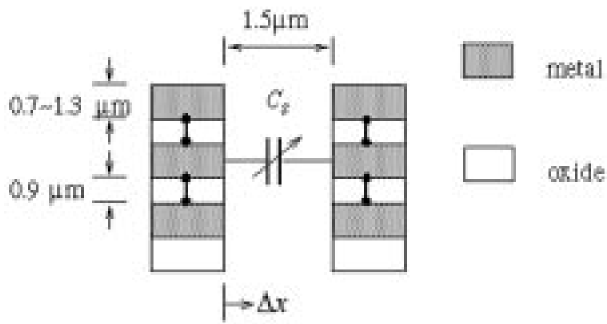

Fig. 8. Cross section of sidewall capacitor between fingers. The left finger (rotor) can move toward the right finger (stator) as indicated by Δx. Metal layers in each finger are shorted by vias which are shown as short wires.

electrode. Forty differential sensing comb fingers have length of 55 μm and gap, $g = 1.5$ μm. Using the simple parallel-plate capacitor model, the capacitance between each pair of fingers is calculated to be about 1.6 fF. The total sensing capacitance, C_s is 64 fF.

Since the resonant frequency of the accelerometer is 8.9 kHz, the displacement sensitivity is only 3.1 nm/G, corresponding to 1.3×10^{-16} F/G change in the capacitance. This extremely small capacitance is challenging to measure, because the incremental capacitance change is much less than the parasitic capacitance C_p, which includes the routing parasitic capacitance of 10 fF and the sensing circuit input capacitance around 110 fF. To decrease the parasitic capacitance, the high-impedance node fingers are attached at stators instead of rotors to minimize the distance to the circuits. Modeling the sensing capacitor as a parallel-plate capacitor, the electrical signal sensitivity is

$$\frac{V_o}{a} = V_m \cdot \frac{2C_s}{2C_s + C_p} \cdot \frac{1}{g\omega_r^2} \tag{6}$$

where V_m is the modulation voltage of 2 V, g is the gap of 1.5 μm and ω_r is the resonant frequency of $2\pi 8.9$ kHz. The sensitivity is about 2.2 mV/G.

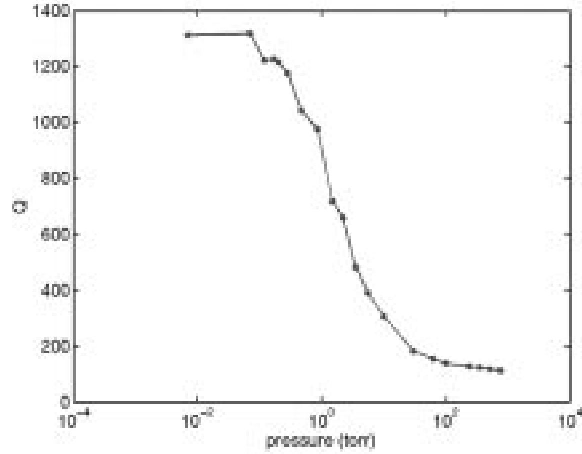

Fig. 9. Quality factor versus pressure.

A potential limitation for the surface micromachined accelerometer is the Brownian noise associated with damping forces. Because the mass is so small, it will be agitated by the collision with air molecules. According to the Nyquist's relation [13] in thermal equilibrium, the spectral density of fluctuation force acting on the device is

$$\frac{F^2}{\Delta f} = 4k_B T b \tag{7}$$

where k_B is the Boltzman constant. The device experiences equivalent noise acceleration

$$\frac{a^2}{\Delta f} = \frac{4k_B T b}{m^2} = \frac{4k_B T \omega_r}{mQ}. \tag{8}$$

For this accelerometer prototype, the model values are $m = 0.57$ μg, $\omega_r = 56$ krad/s, $Q = 24$ (measured), giving an equivalent noise acceleration of approximately 6.9 μG/$\sqrt{\text{Hz}}$ at room temperature. The noise performance can be improved by increasing the mass, which is limited by the dimensions of the microstructure.

Decreasing pressure will significantly boost the quality factor. However the mechanical internal damping will limit this improvement. This damping is related to energy loss from material deformation and internal stress. Measured quality factor with pressure for a similar but smaller (110 μm by 100 μm) CMOS micromachined structure is shown in Fig. 9. The quality factor is extracted from the peak in the electrostatically actuated mechanical frequency response as $Q = \omega_r/\Delta\omega$, where $\Delta\omega$ is the -3 dB bandwidth of the peak. The internal damping dominates at low pressure which causes the Q to saturate at around 1200. The quality factor at low pressure is much less than that of polysilicon and silicon microstructures which have been reported of Q over 80 000 [14].

IV. Electronic Design

The primary challenge in the design of the interface circuits is detecting extremely small capacitance. An interface buffer with low input capacitance is shown in Fig. 10. The capacitive bridge dc bias is set by two small transistors (*M3* and *M4*) working in the subthreshold range. They exhibit large resistance with

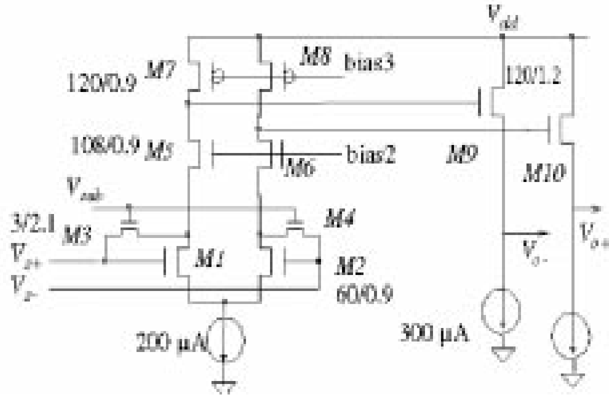

Fig. 10. Differential interface circuit.

negligible source to drain capacitance. The cascode topology has low input capacitance.

Since the system noise level is dominated by the first stage, an input stage with large gain is essential to the system performance. Simulation shows the input sensing buffer has a gain of 80 and bandwidth of 5 MHz with 10 pF capacitance load. No common-mode feedback circuit is needed.

Since the input signal is modulated with a sine wave at a relatively high frequency of 2 MHz, the electronic flicker noise is out of the bandwidth of interest. Therefore, the thermal noise of the transistors is the main source of electronic noise and its spectral density is given by

$$\frac{v^2}{\Delta f} = 4k_BT\left(\frac{2}{3}\right)\frac{1}{g_m}. \tag{9}$$

The sensing buffer has a referred input noise of

$$\frac{v^2}{\Delta f} = 4k_BT\left(\frac{2}{3}\right)\frac{1}{g_{m1}^2}\left[2g_{m1} + 2g_{m7} + 3\cdot\frac{I_{n3}^2}{4k_BT}\right] \tag{10}$$

where I_{n3} has been derived in [15]

$$I_{n3}^2 = 4k_BT\left(\frac{k_BT}{q}\right)\frac{W_3}{L_3}\,\mu C_d \cdot \exp\left(\frac{1}{n}\frac{q}{k_BT}\left(V_{th0} - V_g'\right) - \frac{1}{2}\frac{q}{k_BT}\psi_F\right) \tag{11}$$

and where Ψ_F is the Fermi level, μ is the low-field mobility, V_{th0} is the transistor threshold voltage, n is a process dependent factor, and C_d and V_g' are the depletion capacitance and gate voltage, respectively, when the surface potential is equal to 1.5 Ψ_F. Practically, it is difficult to extract the noise of the I_{n3}. A SPICE simulation shows that noise contribution of I_{n3}^2 is 1000 times smaller than other transistor noise and can be neglected. The sensing buffer is simulated to have a referred input noise of 12 nV/$\sqrt{\text{Hz}}$. Considering the sensitivity of the sensor is 2.2 mV/G, the equivalent circuit noise is about 5.4 μG/$\sqrt{\text{Hz}}$.

The force-balance [16] topology improves the linear range of the accelerometer. It counters any impeding deflection due to acceleration and servos the device back to its null position. The feedback force is generated by separate electrostatic actuators, which have the same structure as the sensing fingers. Enabled by the multilayer routing through the springs, the actuator fingers are biased at the symmetric power rail voltages in the system (V_{dd} and V_{ss}) as shown in Fig. 11. The separate fingers for sensing and actuating eliminate any feedthrough between the driving and sensing signals.

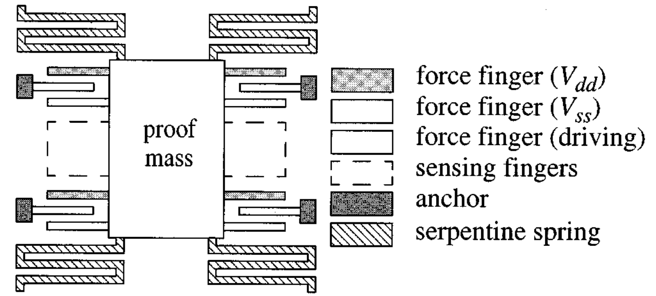

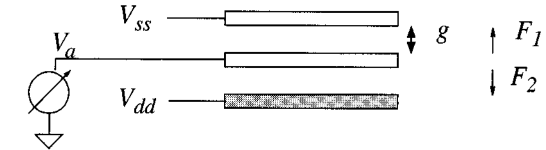

(a)

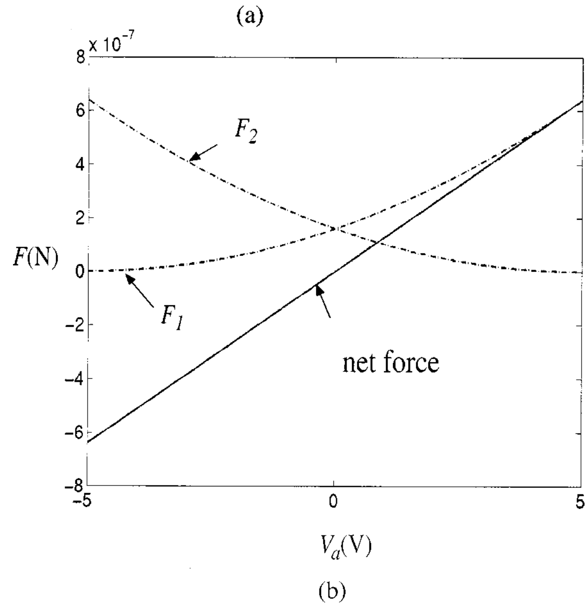

(b)

Fig. 11. (a) Differential force fingers and actuators on the sensor. (b) Electrostatic force linearization.

Because the electrostatic force always attracts the two electrodes of each capacitor, the two forces, F_1 and F_2 (Fig. 11), act in opposite directions on the actuator fingers. Thus the quadratic terms in the forces are cancelled and the net force is linearized. Since in a closed loop, the displacement is very small, it is reasonable to assume the inner finger is centered. The net force is

$$F = \frac{C_0}{2g}\left[(V_{ss} - V_a)^2 - (V_{dd} - V_a)^2\right] \tag{12}$$

where V_a is the actuating voltage. The net force is linearized and is suitable for linear feedback control. The actuator on the accelerometer is biased at ±5 V and can generate a maximum force of 0.64 μN. With a mass of 0.57 μg, the measurement range is 115 G which is large enough for targeted application range of less than 10 G.

Fig. 12 shows a block diagram of the complete feedback loop. The signal is demodulated using an on-chip analog multiplier.

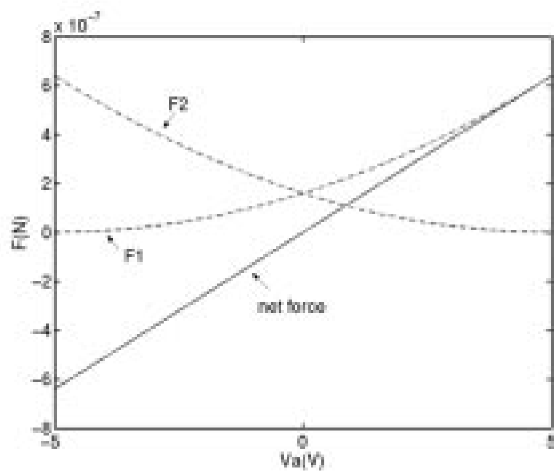

Fig. 12. Schematic of force balance feedback loop.

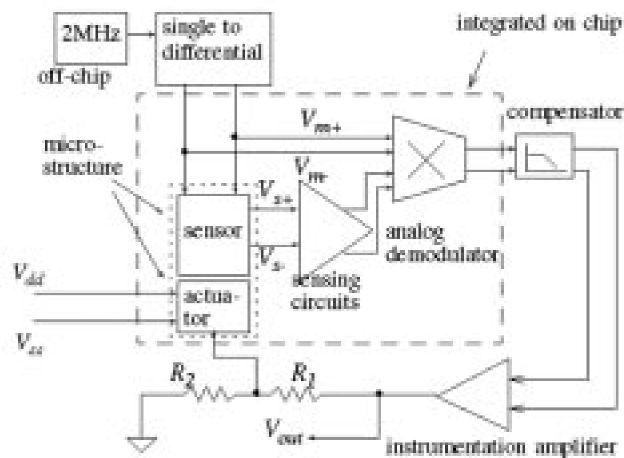

Fig. 13. Displacement versus frequency during self-test.

Since the sensor is a underdamped second-order system, compensation is required for the loop stability. A main pole at 400 Hz is inserted after the demodulation to make the feedback loop stable.

V. Experimental Results

In an initial test, the accelerometer exhibited a visible offset, which mainly came from the lateral curling in the suspension beams. As a result, the middle sensing fingers are not centered. By adjusting the dc bias on the actuator to about 3 V, this offset was nulled. The 3-V dc bias does not affect the actuator linearity with voltage.

In the resonant frequency test, a driving voltage of 3 V_{dc} plus 3 V_{ac} was applied to the self-test actuator on the accelerometer and the motion was measured with the MIT Microvision™ system. Fig. 13 shows the measured displacement versus frequency. The measured resonant frequency is $2\pi 8.9$ kHz.

In the dynamic test, the accelerometer was excited by a 50 Hz 14 G (p–p) sinusoidal acceleration on a Brüel and Kjær vibration table. The waveforms of the output from a reference accelerometer and the output from the CMOS-MEMS accelerometer are compared in Fig. 14. The phase shift is due to the feedback loop

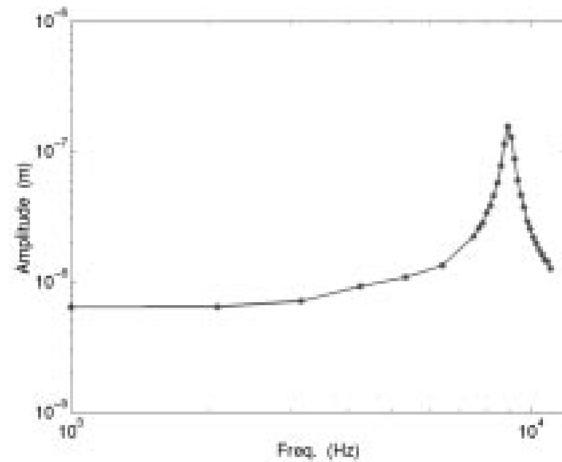

Fig. 14. Waveform of the accelerometer output to a 50 Hz 14 G (p–p) input signal.

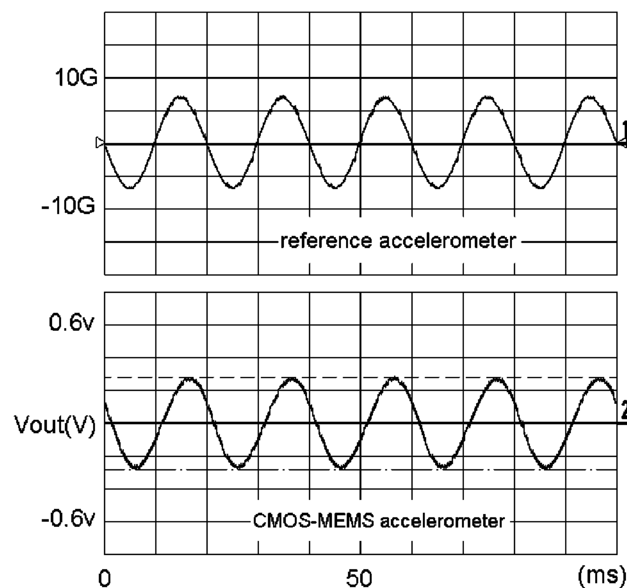

Fig. 15. Spectrum of the accelerometer output when excited by 80 Hz 100 mG acceleration (measured with a 10 : 1 probe).

phase shift plus the phase delay from the mounting mechanical structures including the supporting frame and printed-circuit board.

Fig. 15 shows the spectrum of the output from the accelerometer when excited by an 100 mG acceleration at 80 Hz. The measured noise floor was 1 mG/$\sqrt{\text{Hz}}$, which is much larger than predicted. When the test system was placed on an air table to isolate any test bench vibration, no decrease in the noise was found. In the next test, the accelerometer was put in a vacuum chamber to see the relation between the pressure and the noise. Again, the noise did not decrease at low pressure. Thus we concluded that the electronic noise dominates the system noise performance. There are several possible explanations to the unexpectedly high noise. First, the accelerometer and its conditioning circuits are integrated in a 2.2 mm by 2.2 mm test die, on which there are four other test structures with circuits integrated close to each other. To save the die area, all of them share the same power

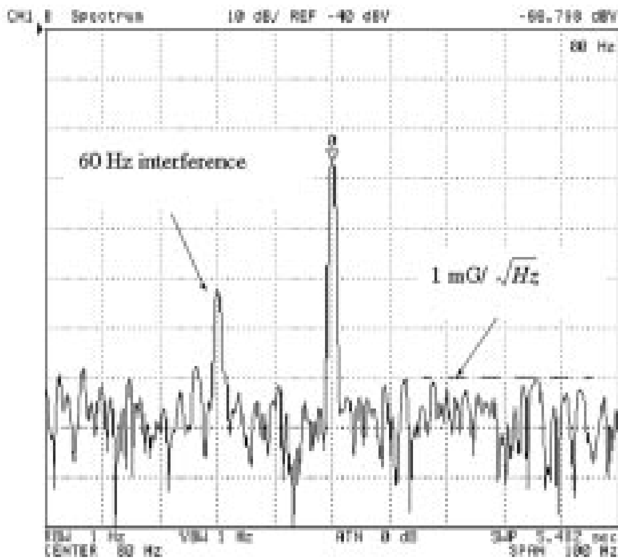

Fig. 16. Accelerometer dynamic linearity (* -) and error (o -) compared to the ideal value.

pads. The other circuits can not be shut down while the accelerometer is being tested. Noise generated by other circuits can be coupled to the accelerometer through the power rails. Second, the measured noise is a composite number of whole system performance. It also includes noise from other parts in the system such as the clock generator, demodulator and amplifier. Third, there may be noise coupled to the high-impedance sense node through leakage current paths on the surface of the microstructures.

Linearity of the accelerometer was measured by applying sinusoidal acceleration at 200 Hz (see Fig. 16). The measured dynamic range of ± 13 g was limited by the maximum output acceleration of the test equipment. Even when the accelerometer experienced a large acceleration shock (>30 G) during a crash test, saturation has not been observed. In the cross-axis sensitivity test, the accelerometer showed a -40 dB attenuation compared to the sensing axis sensitivity.

The accelerometer has been working for over two years and has experienced more than 200 acceleration shock events (>30 G) in demonstrations. No degradation in performance has been observed.

VI. Conclusion

We have reported a functional differential CMOS accelerometer and a complete force-balance feedback test system. It proves the possibility to integrate MEMS accelerometer into a low cost CMOS process and get similar performance as the commercialized polysilicon counterpart. It also shows the advantages of multi-layer routing in CMOS-MEMS structure which gives more design options of electrostatic actuators and capacitive sensors.

Acknowledgment

The authors would like to thank X. Zhu for performing the device release processes.

References

[1] M. Parameswaran, H. P. Baltes, L. Ristic, A. C. Dhaded, and A. M. Robinson, "A new approach for the fabrication of micromechanical structures," *Sens. Actuators*, vol. 19, no. 3, pp. 289–307, 1989.
[2] H. P. Baltes, O. Paul, and O. Brand, "Micromachined thermally based CMOS microsensors," *Proc. IEEE*, vol. 86, pp. 1660–1678, Aug. 1998.
[3] M. J. Syrzycki, L. Carr, G. H. Chapman, and M. Parameswaran, "A wafer scale visual-to-thermal converter," *IEEE Trans. Comp. Hybrids, Manuf. Technol.*, vol. 16, no. 7, pp. 665–673, 1993.
[4] E. J. J. Kruglick, B. A. Warneke, and K. S. J. Pister, "CMOS 3-axis accelerometers with integrated amplifier," in *Proc. IEEE MEMS Workshop*, Heidelberg, Germany, Jan. 25–29, 1998, pp. 631–636.
[5] Analog device ADXL210 accelerometer datasheet. [Online]. Available: http://www.analog.com/pdf/ADXL202_10_b.pdf.
[6] G. K. Fedder, S. Santhanam, M. L. Reed, S. C. Eagle, D. F. Guillou, M. S.-C. Lu, and L. R. Carley, "Laminated high-aspect-ratio micro-structures in a conventional CMOS process," *Sens. Actuators*, vol. A57, no. 2, pp. 103–110, 1996.
[7] X. Zhu, D. W. Greve, R. Lawton, N. Presser, and G. K. Fedder, "Factorial experiment on CMOS-MEMS RIE post processing," in *Proc. 194th Electrochemical Society Meeting, Symposium on Microstructures and Microfabricated Systems IV*, vol. 98-14, Boston, MA, Nov. 1–6, 1998, pp. 33–42.
[8] M. Lu, X. Zhu, and G. K. Fedder, "Mechanical property measurement of 0.5-mm CMOS microstructures," in *Proc. MRS 1998 Spring Meeting., Symposium N: Microelectromechanical Structures for Materials Research*, San Francisco, CA, Apr. 13–17, 1998.
[9] G. Zhang, H. Xie, L. E. de Rosset, and G. K. Fedder, "A lateral capacitive CMOS accelerometer with structural curl compensation," in *Proc. IEEE Micro Electro Mechanical Systems Workshop (MEMS'99)*, Orlando, FL, Jan. 17–21, 1999, pp. 606–611.
[10] H. Lakdawala and G. K. Fedder, "Analysis of temperature-dependent residual stress gradients in CMOS micromachined structures," in *Proc. 10th International Conference on Solid State Sensors and Actuators*, Sendai, Japan, June 1999, pp. 526–529.
[11] H. Luo, G. K. Fedder, and L. R. Carley, "An elastically gimbaled CMOS-MEMS gyroscope," in *CD Proc. International Symposium on Smart Structure and Microstructure*, Hong Kong, Oct. 19–22, 2000, B1-2, pp. 1–6.
[12] M. S.-C. Lu, X. Zhu, and G. K. Fedder, "Mechanical property measurement of 0.5μm CMOS microstructures," in *Proc. Material Research Society (MRS) 1998 Spring Meeting, Symposium on Microelectromechanical Structures for Materials Research*, San Francisco, CA, Apr. 13–17, 1998.
[13] C. Kittel, *Elementary Statistical Physics*. New York: Wiley, 1958.
[14] C. T.-C. Nguyen and R. T. Howe, "Quality factor control for micromechanical resonators," in *Tech. Dig. IEEE International Electron Devices Meeting*, San Francisco, CA, Dec. 14–16, 1992, pp. 505–508.
[15] K. K. Hung, P. K. Ko, and C. Hu, "A physics-based MOSFET noise model for circuit," *IEEE Trans. Electron Devices*, vol. 37, no. 5, May 1990.
[16] K. H.-L. Chau, S. R. Lewis, Y. Zhao, R. T. Howe, S. F. Bart, and R. G. Marcheselli, "An integrated force-balance capacitive accelerometer for low-g applications," *Sens. Actuators, Phys. A*, vol. 54, pp. 472–476, 1996.
[17] G. K. Fedder, "Simulation of microelectromechanical systems," Ph.D. dissertation, EECS, Univ. California, Berkeley, 1994.

Hao Luo received the B.E. degree from Tsinghua University, Beijing, China, in 1994 and the M.S. degree from Carnegie Mellon University, Pittsburgh, PA. He is currently pursuing the Ph.D. degree at the Electrical and Computer Engineering Department at Carnegie Mellon University (CMU), Pittsburgh, PA.

He first worked as a circuit design engineer for two years in Beijing. In 2000, he joined the CMU prize winning team in the nationwide Copper Challenge Design competition held by SRC. His current research interests include MEMS sensor and interface circuit design, and mixed-signal circuit design.

Gang Zhang received the B.E. degree in electronics engineering from Tsinghua University, Beijing, China, in 1994 and the M.S. degree in electrical and computer engineering from Carnegie Mellon University, Pittsburgh, PA, in 1998, where he is currently working toward the Ph.D. degree in RF circuit design and CAD.

Between 1996 and 1998, he worked on first-generation CMOS MEMS accelerometers. Between 1998 and 2000, he worked with Motorola, Inc., AZ, on analog signal conditioning and interface circuits for integrated sensors. Since June 2001, he has been working with Neolinear, Inc., Pittsburgh, on RF circuit design, electrical, and physical synthesis.

L. Richard Carley (F'97) received the S.B., M.S., and Ph.D. degrees from the Massachusetts Institute of Technology (MIT), Cambridge, in 1976, 1978, and 1984, respectively.

In 1984, he joined Carnegie Mellon University (CMU), Pittsburgh, PA, and in 1992, he was promoted to the rank of Full Professor of Electrical and Computer Engineering. In March 2001, he became the STMicroelectronics Professor of Engineering at CMU. He was the Associate Director for Electronic Subsystems for the Data Storage Systems Center (an NSF Engineering Research Center at CMU) from 1990 to 1999. He has worked for MIT's Lincoln Laboratories and has acted as a consultant in the areas of analog and mixed analog/digital circuit design, analog circuit design automation, and signal processing for data storage for numerous companies, e.g., Hughes, Analog Devices, Texas Instruments, Northrop Grumman, Cadence, Sony, Fairchild, Teradyne, Ampex, Quantum, Seagate, and Maxtor. He was the principal circuit design methology architect of the CMU ACACIA analog CAD tool suite, one of the first top-to-bottom tool flows aimed specifically at design of analog and mixed-signal ICs. He was also a Co-Founder of NeoLinear, a Pittsburgh-based analog design automation tool provider; and IC Mechanics, a Pittsburgh-based MEMS sensor IC manufacturer. He has been granted 10 patents, authored or co-authored over 120 technical papers, and authored or co-authored over 20 books and/or book chapters.

Dr. Carley has won several awards, the most noteworthy of which are the Presidential Young Investigator Award from the National Science Foundation in 1985, being made a Fellow of the IEEE in 1997 for contributions to analog circuit design and analog design automation, and winning a Best Technical Paper Award at the 1987 Design Automation Conference (DAC). This DAC paper on automating analog circuit design was also selected for inclusion in "25 years of Electronic Design Automation: A Compendium of Papers from the Design Automation Conference," a special volume, published in June of 1988, including the 77 papers (out of over 1600) deemed most influential over the first 25 years of the Design Automation Conference. He was awarded the Guillemin Prize for best Undergraduate Thesis in the Electrical Engineering Department at MIT.

Gary K. Fedder received the B.S. and M.S. degrees in electrical engineering from the Massachusetts Institute of Technology (MIT), Cambridge, in 1982 and 1984, respectively. In 1994, he received the Ph.D. degree from the University of California, Berkeley, where his research resulted in the first demonstration of multimode control of a underdamped surface-micromachined inertial device.

He is an Associate Professor at Carnegie Mellon University (CMU), Pittsburgh, PA, holding a joint appointment with the Department of Electrical and Computer Engineering and The Robotics Institute. From 1984 to 1989, he worked at the Hewlett-Packard Company on circuit design and printed-circuit modeling. His present research interests include microsensor and microactuator design and modeling, integrated MEMS manufactured in CMOS processes and structured design methodologies for MEMS.

Dr. Fedder received the 1993 AIME Electronic Materials Society Ross Tucker Award, the 1996 Carnegie Institute of Technology G.T. Ladd Award, and the 1996 NSF CAREER Award.